Experimental and analytical analysis

Prestressed steel fibre reinforced concrete beams

Despite the wide research and the continuously increasing structural applications of fibre reinforced concrete (FRC), the use is still restrict-ed with respect to its potentials. This is mainly caused by the lack of international building codes for FRC structural elements and the incom-plete understanding of its complex behaviour. This paper therefore presents the results of an experimental and analytical investigation on the shear capacity of 6 prestressed steel fibre reinforced concrete beams. The beams are subjected to a four-point bending test until failure and the main investigated parameters are the fibre dosage, the amount of prestressing and the amount of shear reinforcement. Both tradi-tional mechanical measurement devices as advanced optical techniques are used.

■ M. De Smedt, K. De Wilder and L. Vandewalle, Building Materials and Building
Technology Section, Department of Civil Engineering, KU Leuven, Belgium ■

Steel fibre reinforced concrete (SFRC) is a cementitious composite material, consisting of a concrete matrix with discrete, randomly dis-tributed steel fibres. SFRC is characterised by an enhanced post-cracking behaviour due to the bridging of crack surfaces by the fibres. Advantages such as an improved ductility and a higher ener-gy absorption capacity, depending on the fibre content and the aspect ratio, are generally accepted nowadays. It is thus currently established that adding steel fibres to the concrete mixture can have a beneficial effect on the overall structural response in both the ulti-mate limit state (ULS) and the serviceability limit state (SLS). However, determining the actual contribution of the steel fibres to the overall shear capacity of large elements still remains open for discussion.

Furthermore, the application of SFRC can be cost- and time-effective by (partially) replacing the conventional reinforcement. The manu-facturing of stirrups and reinforcement cages is time consuming and requires a lot of manual labour. Especially in precast industry, SFRC is of economic interest because of its cost- and time-effectiveness. Since most of the precast structural elements are pretensioned, it is profitable to investigate prestressed SFRC elements, as done in this study.

This paper firstly elaborates the experimental program, with specif-ic attention to the experimental setup and the use of advanced opti-cal measurement methods (i.e. stereo-vision digital image correla-tion and Bragg grated optical fibres). Secondly, the results are pre-sented and compared to analytical predictions according to exist-ing design codes.

Experimental research

Test specimens

Six prestressed beams are made at the local precast manufacturer Ergon nv, Belgium. Each specimen is denoted with the descriptive letter B followed by a number varying from 401 to 406 (refer to Figure 1). All beams have an I-shaped cross section, a length of 7,000 mm and a height of 630 mm. The flange width equals 240 mm whereas the web width equals 70 mm. All specimens are pre-stressed with seven 7-wire low relaxation strands at the bottom and one 7-wire low relaxation strand at the top (nominal diameter of 12.5 mm). All strands of specimens B401-B403 have an initial pre-strain of $7.5 \cdot 10^{-3}$ mm/mm (σ_{p0} equal to 1,488 MPa) whereas the strands of specimens B404-B406 have an initial prestrain of $3.8 \cdot 10^{-3}$ mm/mm (σ_{p0} equal to 750 MPa). Although reducing stress levels below the allowable is uncommon in industry, it is applied to investigate the influence of the prestressing force on the shear capacity while the longitudinal reinforcement ratio remains constant.

Conventional shear reinforcement, consisting of single legged stir-rups (nominal diameter of 6 mm, centre-to-centre distance of 150 mm) is used in beams B401 and B404. Steel fibres (Dramix RC-80/30-CP; length 30 mm, diameter 0.38 mm, tensile strength 3070 MPa) are added to the concrete mixture to replace the convention-al shear reinforcement in the remaining specimens. Beams B402 and B405 are provided with 20 kg/m³ whereas 40 kg/m³ is pro-vided in beams B403 and B406. All specimens are provided with splitting reinforcement at the ends (nominal diameter of 8 mm, cen-tre-to-centre distance of 50 mm) to withstand the gradual develop-ment of the prestressing force over the beam's anchorage length and height. The geometry and reinforcement layout of the present-ed test beams are shown in Figures 2 and 3.
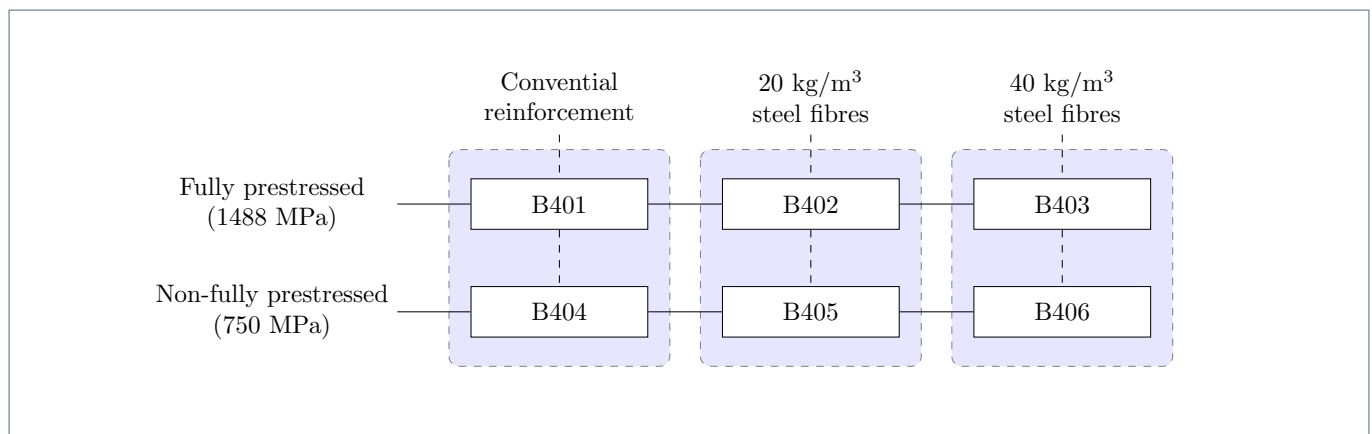
Fig. 1: Overview of the six different test specimens.

■ ir. Maure De Smedt is a PhD student in the Department of Civil Engineering at the KU Leuven, from which she holds BSc (Eng) and MSc (Eng) degrees. After finishing her master thesis on the experimental and analytical analysis of the shear capacity of prestressed steel fibre reinforced concrete beams, she continues her research on steel fibre reinforced concrete by investigating its fatigue loading under tension. maure.desmedt@kuleuven.be

■ Dr.ir.-arch. Kristof De Wilder obtained his doctoral degree at the KU Leuven in 2014 on modelling the shear capacity of prestressed and reinforced concrete beams. His main area of expertise lies in the field of structural modelling, both analytical and numerical, of concrete components. He currently works as a structural design engineer for the Engineering Department of the BESIX Group. kristof.dewilder@kuleuven.be

■ Prof.dr.ir. Lucie Vandewalle is Professor of Civil Engineering in the KU Leuven, from which she holds BSc (Eng), MSc (Eng, 1981) and PhD degrees (1988). Her teaching and research interests are in advanced concrete design and technology, with focus on experimental testing and constitutive modelling of fibre reinforced concrete (FRC) and prestressed concrete. She is convenor of fib (International Federation for structural Concrete) Group 4.1 on fibre reinforced concrete, chairlady of CEN (European Committee for Standardization) TC104/WG11 and member of CEN TC250/SC2/WG1/TG2. lucie.vandewalle@kuleuven.be

Fig. 2: Longitudinal view of the test beams (units in mm; shaded grey indicates steel fibre reinforced concrete; DEMEC points are indicated with o).
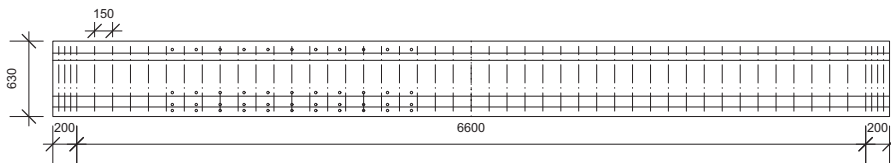
(a) B401 and B404
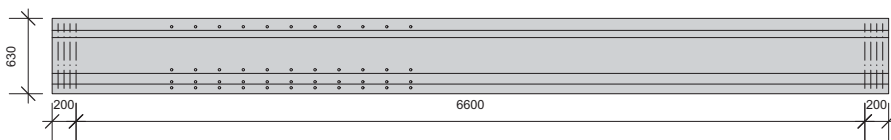
(b) B402, B405 (20 kg/m³) and B403, B406 (40 kg/m³)

Fig. 3: Cross sections and reinforcement layout of the test beams (units in mm; shaded grey indicates steel fibre reinforced concrete).
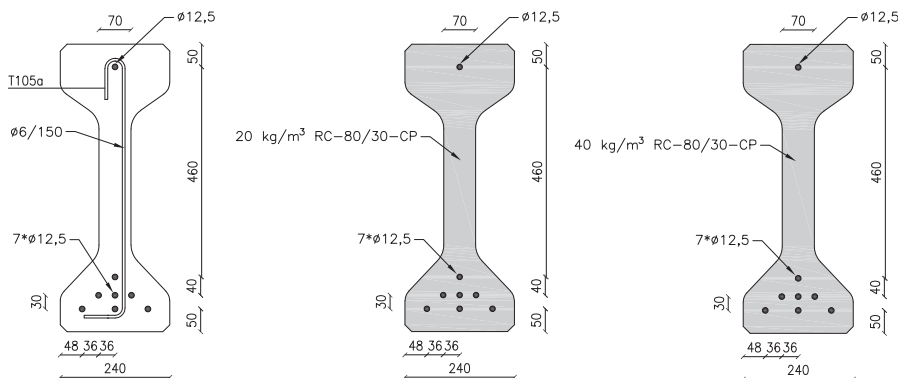
(a) B401 and B404   (b) B402 and B405   (c) B403 and B406

Table 1: Concrete mixture compositions for the presented test beams.

Material	Mixture 1 (B401, B404) Amount [kg/m³]	Mixture 2 (B402, B405) Amount [kg/m³]	Mixture 3 (B403, B406) Amount [kg/m³]
CEM I 52.5 R	368.0	375.3	306.7
Blast furnace slag	0.0	0.0	128.7
Sand 0/2	700.0	700.0	680.7
Limestone gravel 2/12	1,123.0	1,090.7	1,006.0
Water	106.7	107.3	122.7
Limestone filler	130.7	131.3	149.3
High-range water reducer	5.4	5.4	5.6
Steel fibres RC-80/30-CP	0.0	20.0	40.0

Table 2: Experimentally determined material properties for the reported test specimens.

Specimen	$f_{cm,cube}$ (#,s) [MPa]	f_{cm} (#,s) [MPa]	E_{cm} (#,s) [GPa]	$f_{ctm,fl}$ (#,s) [MPa]	ρ_m (#,s) [kg/m³]	Age [days]
B401	79.4 (3, 3.49)	75.6 (3, 0.94)	45.4 (3, 1.89)	9.5 (3, 0.40)	2431 (6, 7.52)	38
B402	65.0 (3, 1.28)	73.8 (3, 7.14)	39.5 (3, 1.05)	5.0 (3, 0.24)	2364 (6, 18.34)	43
B403	67.7 (3, 1.03)	69.7 (3, 4.63)	41.1 (3, 1.21)	5.5 (3, 0.18)	2395 (6, 9.38)	47
B404	97.9 (3, 0.85)	68.1 (2, -)	47.8 (2, -)	5.5 (3, 0.18)	2434 (6, 11.68)	52
B405	78.1 (3, 1.18)	79.4 (3, 3.47)	41.1 (3, 1.07)	4.2 (3, 0.17)	2363 (6, 11.29)	56
B406	89.5 (3, 0.12)	77.4 (3, 12.27)	44.5 (3, 4.59)	5.6 (3, 0.28)	2389 (6, 9.56)	57

# indicates the number of test results, s presents the standard deviation

Table 3: Experimentally determined mean residual flexural tensile strength of B402-B403 and B405-B406.

Specimen	$f_{Rm,1}$ [MPa]	$f_{Rm,2}$ [MPa]	$f_{Rm,3}$ [MPa]	$f_{Rm,4}$ [MPa]
B402	3.32	3.80	3.50	3.10
B403	8.81	8.66	7.97	6.99
B405	4.20	4.46	4.04	3.44
B406	9.92	9.03	7.61	6.39

Table 4: Reinforcement properties.

Reinforcement type	Type	d_s* d_p [mm]	E_s E_p [GPa]	f_{ym} $f_{p0.1m}$ [MPa]	f_{tm} f_{pm} [MPa]	ε_{su} ε_{pu} [%]
Shear reinforcement	Cold worked	6.0	210.0	608	636	2.73
Splitting reinforcement	Cold worked	8.0	203.0	542	603	5.97
Prestressing reinforcement	7-wire strands	12.5	198.0	1737	1930	5.20

*subscript s and p denote conventional respectively prestressing reinforcement types

Fig. 4: Experimentally obtained CMOD-stress curves for the beams with steel fibres
(note: ○ indicates mean residual flexural tensile strengths at CMOD equal to 0.5, 1.5, 2.5 and 3.5 mm).
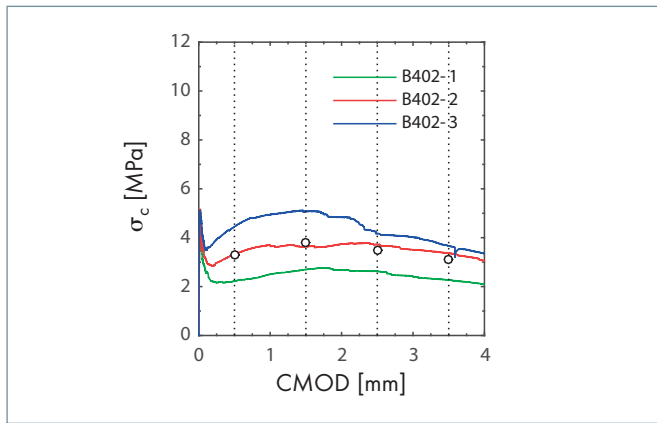
(a) B402 (20 kg/m³)
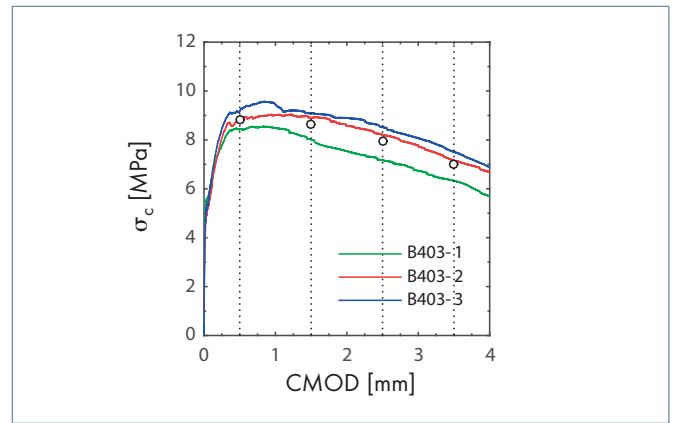
(b) B403 (40 kg/m³)
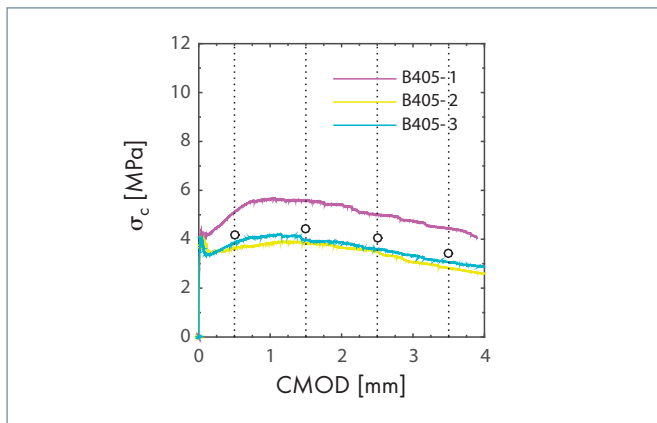
(c) B405 (20 kg/m³)
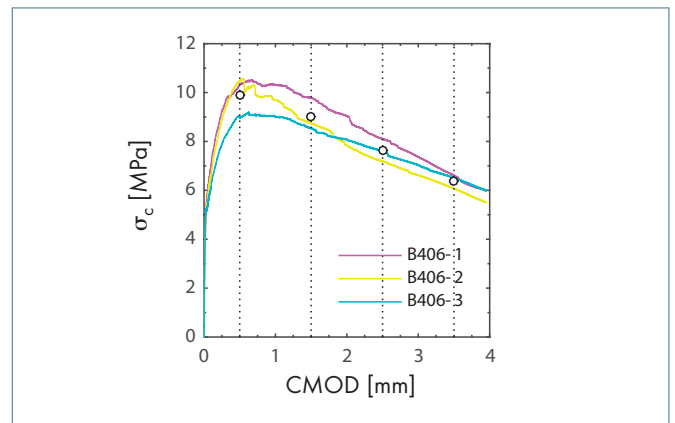
(d) B406 (40 kg/m³)

Materials

A self-compacting concrete mixture is used to cast the presented test specimens, with additional mechanical vibration to ensure a good compaction of beams B402-B403 and B405-B406 with fibres. The mixture properties are listed in Table 1. All three mixtures are designed to have a characteristic cylindrical compressive strength f_{ck} equal to 50 MPa.

All mixtures are made in volumes of 1.5 m³. Together with each beam, three cubes (150 x 150 x 150 mm³), three cylinders (diameter 150 mm, height 300 mm) and three prisms (150 x 150 x 600 mm³) are cast to determine material properties according to the European Standards, namely the mean cube compressive strength $f_{cm,cube}$, the mean cylindrical compressive strength f_{cm}, the mean secant modulus of elasticity E_{cm}, the mean flexural tensile strength $f_{ctm,fl}$ and the residual flexural tensile strength $f_{R,i}$ (with j=1,2,3,4) in case of SFRC. The experimentally determined material properties are listed in Table 2. The mean concrete density ρ_m and the age at the day of testing is also presented in Table 2. Figure 4 shows the measured stress-CMOD (Crack Mouth Opening Displacement) for the adopted concrete mixture with 20 kg/m³ and 40 kg/m³ respectively, measured according to EN 14651. The stress-CMOD curves show the softening behaviour of concrete with 20 kg/m³ steel fibres and the hardening behaviour of concrete with 40 kg/m³ steel

fibres, under bending loads. The derived residual flexural tensile strengths $f_{R,i}$ (with j=1,2,3,4) are presented in Table 3.

The material properties of the reinforcement are summarized in Table 4. Tensile tests were performed on the shear and splitting reinforcement to determine the modulus of elasticity E_s, the yield and ultimate stress, f_{ym} respectively f_{tm}, and the strain at failure ε_{su}. The characteristics of the prestressing strands were taken from the manufacturer.

Experimental setup

The six beams are subjected to a four-point bending test, as schematically shown in Figure 5 and depicted in Figure 6(a). All tests are carried out in load control, using a hydraulic press (Instron, maximum capacity 2.5 MN), following a progressive damage loading scheme. Figure 7(a) shows a typical progressive damage loading scheme as a function of time whereas Figure 7(b) presents the corresponding load-displacement curve obtained from the load-displacement data of the hydraulic press. The first cycle goes to half of the predicted cracking load, the second one up to the predicted cracking load and in the third cycle the load is increased until failure. The loading rate equals to 0.25 kN/s whereas the unloading rate is either equal to 0.25 kN/s (first cycle) or 1.00 kN/s (second cycle). The distance between the supporting points is 5,000 mm.

Fig. 5: Schematic representation of the experimental setup.
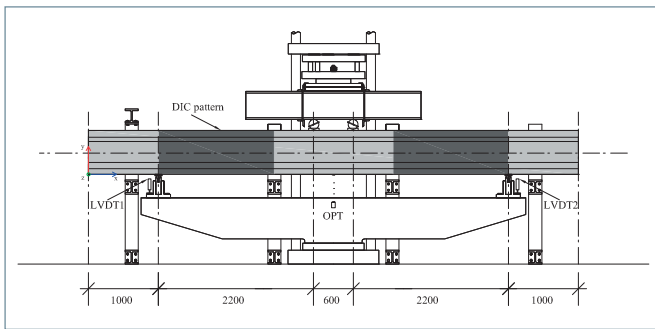
(a) Front view with indication of the measurement methods LVDT, OPT and DIC
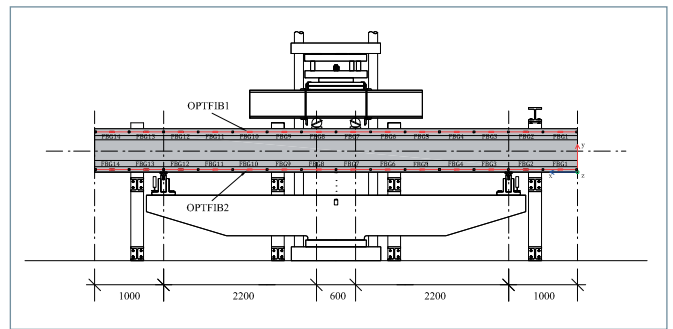
(b) Back view with indication of the optical fibres OPTFIB, mechanical fixing points and Bragg gratings (FBG)

Fig. 6: Experimental setup for the test specimens.

(a) Front view with DIC pattern

(b) Camera setup for DIC measurements

(c) Back view with optical fibres

(d) Mechanically anchored optical fibre

Fig. 7: Typical applied progressive damage scheme as a function of time and corresponding observed shear force-vertical displacement curve (here depicted for specimen B403).
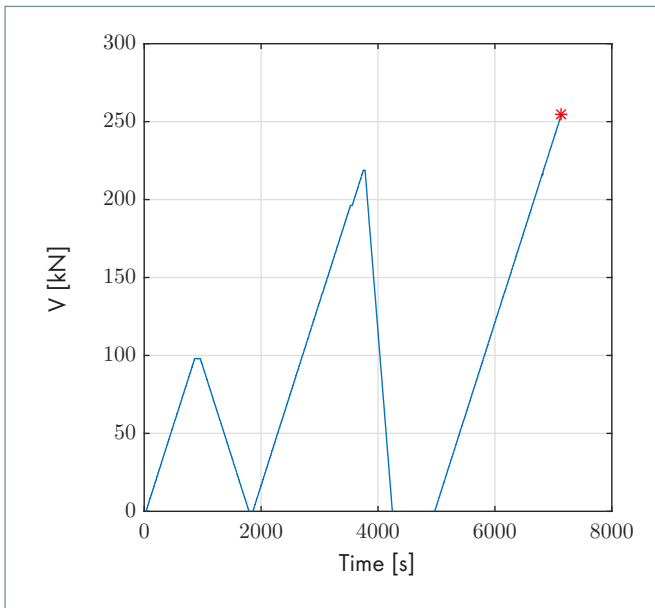
(a) Load pattern
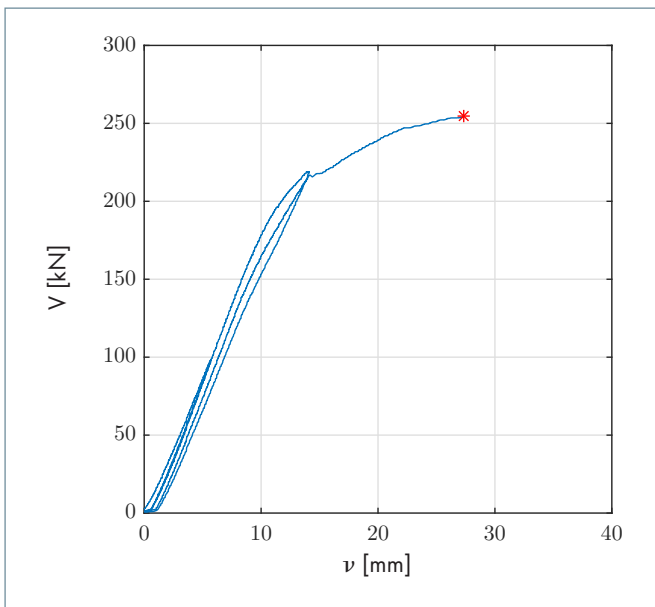
(b) Load-displacement curve

The distance outside the supporting points is therefore equal to 1,000 mm at each end. This allows the authors to study shear outside the length needed for the prestressing force to gradually develop over the beam's anchorage length and height. The shear span a is equal to 2,200 mm for all beams, resulting in a shear span-to-effective depth ratio equal to 3.95, designed to obtain shear failure. Table 5 gives an overview of the investigated parameters per specimen.

Table 5: Overview of the experimental program and the investigated parameters.

Specimen	Type	L [mm]	d [mm]	σ_{p0} [MPa]	a [mm]	a/d [–]	ρ_l [–]	ρ_w* [x 10^{-3}]	V_f [kg/m^3]	$V_{u,exp}$ [kN]
B401	I	7,000	557	1,488	2,200	3.95	0.0167	2.693	0	256.4
B402	I	7,000	557	1,488	2,200	3.95	0.0167	0	20	218.5
B403	I	7,000	557	1,488	2,200	3.95	0.0167	0	40	254.4
B404	I	7,000	557	750	2,200	3.95	0.0167	2.693	0	202.5
B405	I	7,000	557	750	2,200	3.95	0.0167	0	20	164.1
B406	I	7,000	557	750	2,200	3.95	0.0167	0	40	197.4

*shear reinforcement ratio equal to $A_{sw}/(b_w s)$

Adopted measurement techniques

Continuous displacements of all specimens are measured using LVDTs at the supporting points and an optical photoelectric sensor (Baumer Photoelectric OADM 12U6460, resolution $96 \cdot 10^{-3}$ mm) at midspan of the beam, see Figure 5(a). However, if the mechanical behaviour is to be thoroughly understood, more detailed displacement and deformation data in three dimensions is required over the entire loading range. Setups employing the aforementioned measurement devices, rapidly become cumbersome. Therefore, advanced optical measurement techniques are also used to characterize the mechanical response during the applied loading procedure. Two Stereo-vision Digital Image Correlation systems (DIC) are employed to analyse the full-field displacement and deformation field, refer to Figure 5(a). Bragg grated optical fibres (FBG) are used during the experiments on specimens B403 (top flange) and B404 (top and bottom flange) to accurately measure the horizontal strains in the flanges, refer to Figure 5(b).

As an optical and contactless measurement method, the basic principle of DIC is to take images of the undeformed and deformed state of an area of interest and to calculate the displacement by correlating these images. The areas of interest are the shear-critical areas and they are covered with a black and white speckle pattern by using a stencil printing technique, refer to Figure 6(a). Each DIC system consists of two simultaneously capturing CCD 8-bit cameras (AVT Stingray F-201 B; 1,628 by 1,236 pixels resolution) with lenses having a focal length of 12 mm mounted on a tripod, refer to Figure 6(b). The correlation process and post-processing of the data are done by using MatchID 3D.

Strain monitoring with optical fibres engraved with Bragg gratings relies on the analysis of the wavelength spectrum, which is reflected by the Bragg gratings. If a change in length of the fibre occurs, a shift in the reflected wavelength is induced (positive shift is an elongation). Each optical fibre (FOS&S, type SMW-01; based on Draw Tower Grating technology; primary ORMOCER coating) is equipped with 14 FBG sensors with a base length of 500 mm and mechanically fixed into brass anchoring blocks glued on the concrete surface, refer to Figure 6(d). A high resolution FBG interrogator is applied for readouts of wavelengths between 1,525 nm and 1,565 nm.

Experimental results and discussion

In this section, the experimentally observed structural behaviour is reported. Figure 8 shows the observed load-displacement response curves for the tested beams. It clearly shows that all specimens exhibit a profound post-cracking behaviour, even for highly prestressed specimens with a relatively low fibre dosage (refer to specimen B402).
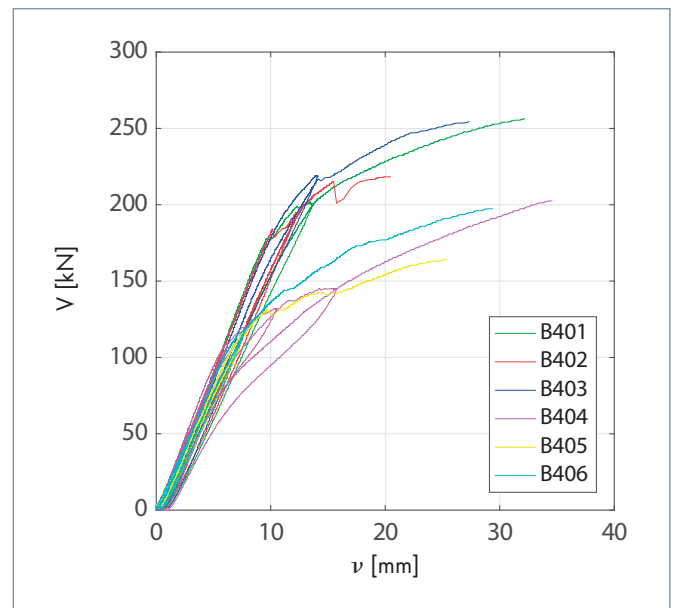
Fig. 8: Experimentally observed load-displacement curves (at the location of the loading point) of the tested beams.

All specimens were designed to fail in shear. Indeed, a shear failure mode, i.e. diagonal tension failure (S-DT), was encountered for all specimens. Severe web cracking led to yielding and rupture of the shear reinforcement elements for specimens B401 and B404. The steel fibres of specimens B402-B403 and B405-B406 were found to be pulled out of the concrete matrix at the failure surface. Fibre rupture was not encountered during the experiments. The experimentally observed failure mode for the specimens is presented in Figure 9 and the corresponding failure load $V_{u,exp}$ is given in Table 5.

Typically obtained experimental results of the DIC measurement and the FBGs are presented in Figure 10 and 11 respectively. The DIC results clearly show the development of a shear crack in the horizontal and vertical displacement field and allow measuring the crack widths during the loading procedure. The FBG results show the shortening of the top flange due to compression and that the beam remains uncracked in the first loading cycle. The first cracks appear in the midspan of the beam at FBG7&8, i.e. cracking due to bending, while the largest cracks develop in the shear-critical area (FBG5&10 and FBG4&11).

Fig. 9: Experimentally observed shear failure mode of the tested beams.

The experimentally obtained failure loads of the SFRC beams ($V_{u,exp}$) are compared to the predictions of the shear capacity ($V_{u,pred}$) according to several analytical models for SFRC, i.e. the DRAMIX Guideline, the RILEM Method, the CNR model, the Model Code 2010 and the model proposed by Soetens [1]. The results, refer to Figure 12, show an underestimation of the predicted shear capacities of all the models, which leads to a safe design. The disadvantage is that some results are already very safe (maximum experimental-to-predicted ratio of 1.58), although all partial safety factors are omitted and average material properties are used.
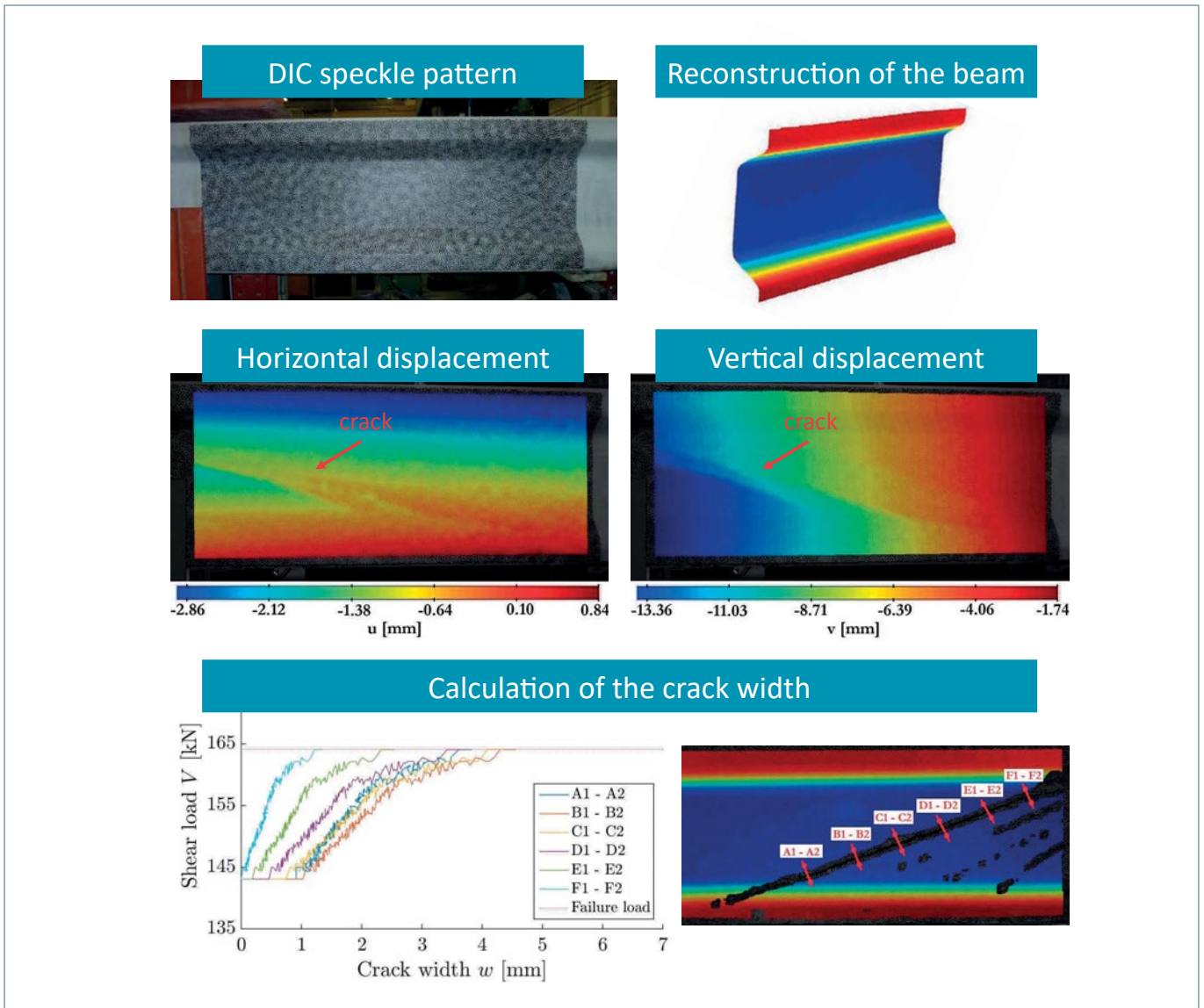
Fig. 10: Typically observed results obtained from DIC: reconstruction of the beam in unloaded state; horizontal and vertical displacement field for the left side of B401 at a load of 236 kN; measuring of the crack widths of B405 by placing virtual extensometers over the crack in the DIC measurements.
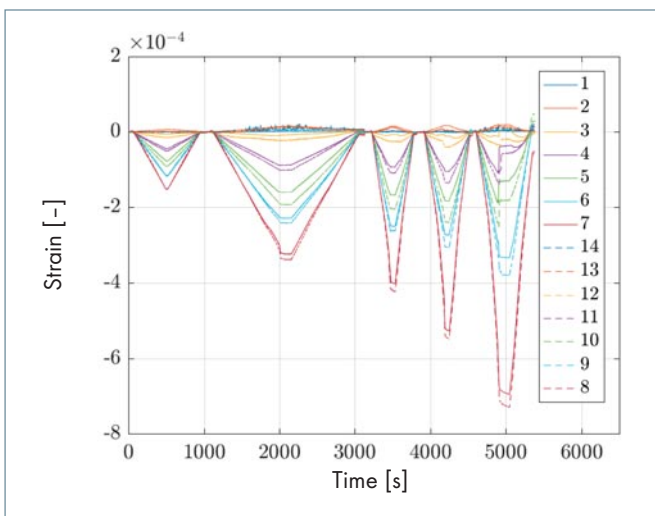
Fig. 11: Typically observed results obtained from FBGs: symmetrical strain data of the top flange of beam B404 for five loading cycles.
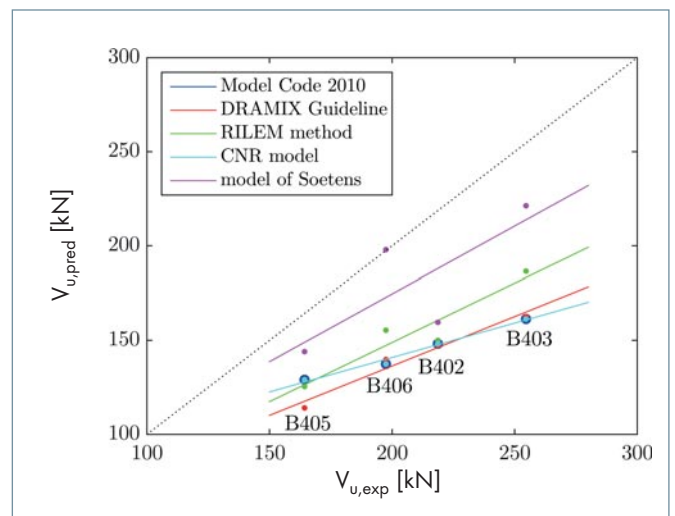
Fig. 12: Experimental failure loads compared to the analytical predictions according to different analytical models of the shear capacity of SFRC.

Therefore, the design values of the shear capacity will be even safer and could be too conservative, leading to expensive designs.

Finally, the following conclusions concerning the experimental results (Table 5) and the calculation procedures (Figure 12) can be made:

- As expected, an increased prestressing force, with a constant longitudinal reinforcement ratio, results in an increased shear capacity, an extended elastic region and a lower inclination of cracks for specimens with (B401 – B404) and without (B402 – B405, B403 – B406) shear reinforcement. An increased amount of fibres, for specimens with a constant prestressing force and without shear reinforcement, also results in a higher shear capacity, and a larger post-cracking behaviour with a more gradual energy dissipation (B402 – B403, B405 – B406).
- Both the experimental results and the predictions show that the shear capacities of the specimens with shear reinforcement and the specimens with 40 kg/m³ steel fibres are comparable (B401 – B403, B404 – B406). It can be concluded that replacing the amount of shear reinforcement $\rho_w = 2.693 \cdot 10^{-3}$ by 40 kg/m³ of steel fibres results in a similar shear capacity for the tested specimens. Although all specimens failed due to shear, a clear distinction has to be made between the failure development of beams with shear reinforcement and beams with fibres. Multiple cracks occur for elements B402-B403 and B405-B406 (with fibres) whereas one major crack where all the deformation is localized is observed for beams B401 and B404 (with conventional shear reinforcement). Failure of specimens B401 and B404 is very brittle, highly energy releasing and occurs without the possibility of redistribution of internal forces. Failure of fibre reinforced specimens on the contrary is more ductile, even though a shear failure mode is observed, and redistribution of internal forces is to some extent possible.
- The predicted failure loads are always an underestimation of the experimentally observed ones. The underestimation (the ratio $V_{u,exp}/V_{u,pred}$) increases for a higher prestressing force (B402 – B405, B403 – B406). The influence of the prestressing force is not completely correctly estimated in the different models, especially for higher prestressing values. In some models, the influence of a higher amount of steel fibres is better estimated and vice versa for other models. The contribution of the steel fibres still remains discordant and rather unknown correctly.

In further research a more fundamental investigation of the discrepancy between the experimental and predicted failure loads can be made, especially the influence of the amount of prestressing force or fibre dosage.

Conclusions

This paper presented the results of six I-shaped prestressed steel fibre reinforced concrete beams subjected to a four-point bending test until failure. The main investigated parameters were the amount of prestressing, the amount of shear reinforcement and the fibre dosage. Besides traditional mechanical measurement systems, stereo-vision digital image correlation and Bragg grated optical fibres were used. The experimental failure loads were compared to analytical predictions based on different models. Based on the work presented, it is concluded that the influence of prestressing force or fibre dosage remains difficult to take into account and that all analytical models underestimate the shear capacity of SFRC.

Acknowledgements

■ **Literature**

[1] De Smedt, M., Experimental and analytical analysis of the shear capacity of prestressed steel fibre reinforced concrete beams. Master thesis, Department of Civil Engineering, KU Leuven, 2016.